ARTICLE

Bio-Based Trivalent Phytate: A Novel Strategy for Enhancing Fire Performance of Rigid Polyurethane Foam Composites

Bing Zhang[1], Sujie Yang[1], Mengru Liu[1], Panyue Wen[2], Xiuyu Liu[1], Gang Tang[1,*] and Xiangrong Xu[3,4,*]

[1]School of Architecture and Civil Engineering, Anhui University of Technology, Ma'anshan, 243002, China

[2]State Key Laboratory of Fire Science, University of Science and Technology of China, Hefei, 230026, China

[3]School of Mechanical Engineering, Anhui University of Technology, Ma'anshan, 243002, China

[4]University of Belgrade, Belgrade, 11120, Serbia

*Corresponding Authors: Gang Tang. Email: tanggang@ahut.edu.cn; Xiangrong Xu. Email: xuxr@ahut.edu.cn

ABSTRACT

Biomass phytic acid has potential flame retardant value as the main form of phosphorus in plant seeds. In this study, phytate-based flame retardants aluminum phytate (PA-Al) and iron phytate (PA-Fe) were synthesized and characterized. Subsequently, they were introduced into rigid polyurethane foam (RPUF) as flame retardants by one-step water-blown method. The results indicated that RPUF/PA-Fe30 exhibited the highest char residue of 22.1 wt%, significantly higher than 12.4 wt% of RPUF. Cone calorimetry analysis showed that the total heat release (THR) of RPUF/PA-Al30 decreased by 17.0% and total smoke release (TSR) decreased by 22.0% compared with pure RPUF, which were the lowest, demonstrating a low fire risk and good smoke suppression. Thermogravimetric analysis-Fourier transform infrared spectrometer (TG-FTIR) implied the release intensity of flammable gases (hydrocarbons, esters) and toxic gases (isocyanate, CO, aromatic compounds, HCN) of composites was significantly reduced after the addition of PA-Fe. The analysis of char residue indicated that the RPUF composites formed a dense char layer with a high degree of graphitization after the addition of PA-Al/PA-Fe, endowing RPUF composites with excellent mass & heat transmission inhibition effect and fire resistance in the combustion process.

KEYWORDS

Bio-based flame retardant; phytic acid salt; rigid polyurethane foam; composites; smoke & toxicity suppression

1 Introduction

In the polyurethane system, rigid polyurethane foam (RPUF) has the advantages of convenient construction, low thermal conductivity, good compression resistance and low density, so it is widely used in building insulation, petrochemicals, transportation and household appliances [1–5]. However, RPUF is highly combustible and releases large amounts of heat in a short time because of its porous structure and organic skeleton. When the temperature rises to the decomposition temperature, RPUF begins to pyrolyze into oligomers, producing various combustible gases that react with oxygen to further intensify the combustion process. At the same time, the combustion of RPUF will produce much smoke and toxic gases [6,7]. In recent years, fire accidents caused by the ignition of RPUF occur frequently. Therefore,

how to modify the flame retardant of RPUF composites and effectively reduce the toxic flue gas in the combustion process has become a prominent problem to be solved.

Adding flame retardants directly into polymer is the most effective method to modify the polymer. In past few decades, researchers have developed various flame retardants for flame retardant modification of various polymers. These flame retardants can be divided into halogen-based flame retardants and halogen-free flame retardants according to whether they contain halogen elements. Although halogen-containing flame retardants present excellent fire retardant efficiency, it often results in the production of variety corrosive substances and toxic gases during combustion, which was gradually abandoned by people [8–10].

In recent years, biomass flame retardants have been widely concerned by the industrial and academic circles with the popularity of the environmental protection concept [11–13]. Yang et al. [14] used malic acid and 1, 6-hexanediol as raw materials to synthesize a series of biomass multi-functionality polyester polyols (MAP) with different alcohol-acid ratios, which were used to prepare RPUF composites. It was indicated that MAP significantly reduced the thermal conductivity of the composites with uniform cell structures. The thermal conductivity of RPUF-1.8 was only 0.019 W/(m·K), which was approximately 35% lower than that of RPUF-4110. At the same time, the char residue at 700°C of RPUFs based on MAP increased in accordance with the increase of MAP alcohol-acid loading, indicating the possibility that MAP could replace petrochemical polyols. Gao et al. [15] prepared liquefied lignin-based polyol (LBP), which was combined with organic modified layered double hydroxide (OLDH), microencapsulated ammonium polyphosphate (MAPP) and commercial flame retardant Polyols (FRP) to prepare halogen-free flame retardant rigid polyurethane foam nanocomposites. Compared with RPUF, the LOI of modified RPUF composites increased from 19 to 28.1 vol%, and the average heat release rate (avHRR) and total smoke release (TSR) of the nanocomposite were decreased by 48.0% and 50.7%, respectively. Septevani et al. [16] found that bio-based polyols prepared by liquefaction of palm kernel oil-based polyols could be used as renewable materials for the synthesis of rigid polyurethane foams, and polyurethane foams with excellent mechanical and thermal insulation properties could be obtained. Tsuyumoto et al. [17,18] coated RPUF with the mixture of starch and amorphous sodium polyborate (SPB), and the composites exhibited high retardant performance. When hydroxyethyl cellulose, carboxymethyl cellulose, glucomannan, gellan gum and 2-hydroxypropyl guar gum (HPG) were used to replace starch, the flame retardant performance of the composites was further improved. However, most studies focus on thermal hazards, while less attention is paid to the non-thermal hazards of RPUF composites. It should be clear that the casualties in fire mainly come from non-thermal hazards.

Phytic acid (PA) as the main form of phosphorus that exists in oil crops, cereals and legume is a natural, environmentally friendly and biodegradable saturated biological base acid. The development of synergists is relatively simple compared with the synthesis of new flame retardants. In previous studies, phytic acid metal salts have good smoke suppression and toxicity reduction effects, effectively reducing the non-thermal hazard of composites. In this work, two biobased flame retardants, aluminum phytate (PA-Al) and ferric phytate (PA-Fe) were prepared to modify RPUF. This not only improves the effect of high content flame retardant on the matrix, but also reduces the cost to a certain extent. As an organic acid, PA is helpful to improve the dispersion performance of its derivatives in the polymer matrix. At the same time, the six phosphate groups in PA have the strong chelating ability and can be complexed with metal ions [19,20]. In addition, phytic acid is biomass with high phosphorus content, enhancing the flame retardant properties of polymers by promoting their carbonization [21]. On this basis, SEM-EDS, thermal conductivity tester, density measurement, thermogravimetric analysis, cone calorimetry, TG-FTIR and Raman spectroscopy were used to investigate the effects of PA-Al/PA-Fe on the physical properties, thermal stability, pyrolysis gas products and combustion characteristics of RPUF composites.

2 Experimental Section

2.1 Experimental Materials

Polyether polyol (LY-4110) and triethylene diamine (A33%, 33%) were purchased by Jiangsu Lvyuan New Material Technology Co., Ltd., China, Polymethylene polyphenyl polyisocyanate (PAPI) was provided by Wanhua Chemical Group Co., Ltd., China, Dibutyltin dilaurate (LC) was purchased from American Air Chemical Co., Ltd., Silicone surfactant (AK-8805) was provided from Jining Hengtai Chemical Co., Ltd., China, Triethanolamine (TEOA), sodium hydroxide (NaOH), $Al_2(SO_4)_3 \cdot 18H_2O$ and $Fe(NO_3)_3 \cdot 9H_2O$ were obtained from China Sinopharm Chemical Reagent Co., Ltd., and phytic acid (PA: 70 wt% aqueous solutions) was purchased from Aladdin biochemical reagent Co., Ltd., Distilled water was made in the laboratory.

2.2 Preparation of Phytate Metal Salt

0.04 mol $Fe(NO_3)_3 \cdot 9H_2O$ (16.16 g) and 250 ml distilled water were added to a 1000 ml beaker, respectively, and stirred until completely dissolved. 9.43 g PA solution (equal to 0.01 mol) was mixed with 250 ml distilled water and dropped it into $Fe(NO_3)_3 \cdot 9H_2O$ solution with a constant pressure dropping funnel. Moreover, the pH value of the solution was adjusted to 7–8 with 2.5 mol/L NaOH and reacted at 80°C for 1 h. Then, the mixture was centrifuged to obtain precipitate, which was washed by deionized water for 3 times and drying at 80°C for 12 h, obtaining yellow iron phytate (PA-Fe). Aluminum phytate (PA-Al, white) was prepared as a similar strategy (Scheme 1).
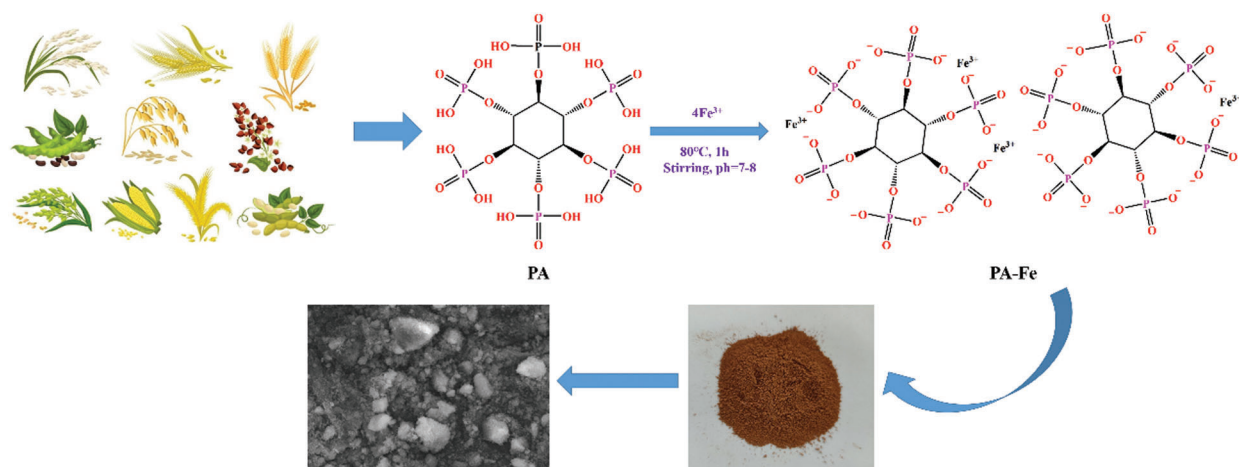

Scheme 1: Synthesis route of phytate metal salt (taking PA-Fe as an example)

2.3 Preparation of RPUF Composites

As shown in Scheme 2, RPUF composites were prepared by one-step water-blown method, with raw materials as shown in Table 1. Except for PAPI, added all the materials were added to a 1000 ml plastic beaker, which was stirred with a high-speed mixer. Then, PAPI was quickly poured into the plastic beaker. The mixture was stirred for about 10 s and turned white with bubbles escaped. Quickly poured it into the mold for foaming. Then putted the sample into an oven, cured it at 80°C for 6 h. Finally, it was cooled at room temperature for 24 h and cut it according to the experiment.

2.4 Testing and Characterization

Fourier transform infrared (FTIR) spectra of PA-Al/PA-Fe powders were performed by Nicolet 6700 FTIR spectrometer (USA) with transition mode and the scanning range was set at 4000–400 cm^{-1}.
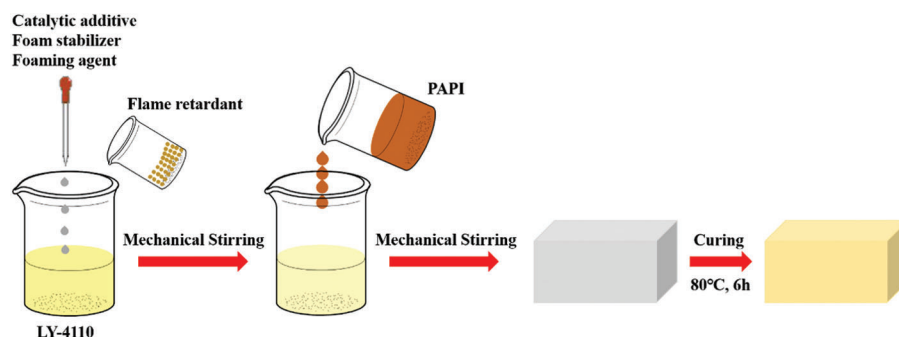
Scheme 2: Preparation diagram of RPUF composites

Table 1: The formulae of RPUF, RPUF/PA-Al and RPUF/PA-Fe composites

Sample	LY-4110/ phr[a]	PAPI/ phr	LC/ phr	AK-8805/ phr	A33/ phr	TEOA/ phr	Water/ phr	PA-Al/ phr	PA-Fe/ phr
RPUF	100	150	0.5	2	1	3	2	0	0
RPUF/PA-Al15	100	150	0.5	2	1	3	2	15	0
RPUF/PA-Al30	100	150	0.5	2	1	3	2	30	0
RPUF/PA-Fe15	100	150	0.5	2	1	3	2	0	15
RPUF/PA-Fe30	100	150	0.5	2	1	3	2	0	30

Note: [a]Parts per hundreds of polyether polyol.

D8ADVANCE X-ray diffractometer (Japan) was applied to test PA-Al/PA-Fe powder, Cu target was used with the power of 3 kW, and test angle of 5–80°. The angle accuracy was ≤0.02°.

Oxford Aztec X-Max 80 energy dispersive X-ray spectrometer (EDS) (UK) combining with SU8220 scanning electron microscope (SEM) (JEOL Ltd., Japan) was applied to scrutinize the cell structure and the morphology of char residues of RPUF composites. The accelerating voltage was 20 kV. The composites were sprayed with a thin layer of conductivity earlier than observation to enhance the conductivity.

Q5000IR (TA instrument, USA) thermal analyzer was used for thermogravimetric analysis (TGA). Nitrogen atmosphere mode was used with a temperature range from room temperature to 800°C and heating rate of 20°C/min.

According to GB/T10297-2015, the thermal conductivity of composites was tested using the TC3000E thermal conductivity instrument (Xi'an Xiaxi Electronic Technology Co., Ltd., China) with sample size of 50 mm × 50 mm × 25 mm. Each group was tested three times, and the average value was reported.

According to GB/T6343-2009, the density of the composites was tested according to the sample mass/ sample volume method. The sample size was 50 mm × 50 mm × 50 mm. Each group was tested for 3 times and the average value was obtained.

According to ASTM-D2863 standard, JF-3 oxygen index instrument (China Jiangning Analytical Instrument Co., Ltd., China) was used to test the limiting oxygen index (LOI) of RPUF composites. The sample size was 127 mm × 10 mm × 10 mm.

According to GB/T2408 standard, the CZF-3 (Nanjing Jiangning District Analytical Instrument Factory, China) horizontal and vertical combustion tester were used to investigate the horizontal combustion grade of composites. The sample size was 125 mm × 13 mm × 10 mm.

Cone calorimeter 6180 (Siemens analyzer) was used to test the combustion properties of composites according to ISO5660-1 standard. The sample size was 100 mm × 100 mm × 25 mm, and the radiation flux was 35 kW/m^2.

Thermogravimetric analysis-Fourier transform infrared spectrometer (TG-FTIR) was conduct by the combination of 170SX Fourier transform infrared spectrometer (Shimadu, Japan) and DT-50 thermogravimetric analyzer (Setaram Instruments, France) to investigate the gaseous products in the degradation process of the composite. 5–10 mg samples were put into an alumina crucible, which was heated from 40°C to 800°C in a nitrogen atmosphere, and the heating rate was 20°C/min.

Raman spectra of char residues were collected by LABRAM-HR Confocal Raman spectrometer (HORIBA Jobin Yvon) with a laser at 514.5 nm laser.

3 Results and Discussion

3.1 Characterization of Phytate Metal Salt

FTIR spectra of PA, PA-Al and PA-Fe were shown in Fig. 1. The bending vibration peaks of water molecules and asymmetric −OH stretching in PA appeared at 1640 and 3410 cm^{-1}, respectively [22]. The absorption peak of P–OH was at 2850 cm^{-1}, and the bending vibration of –CH–CH− appeared at 1398 cm^{-1} [23,24]. The characteristic absorption peaks of stretching vibration of P=O and P–O were at 1126 and 976 cm^{-1}, and the characteristic peaks at 1052 and 1012 cm^{-1} were attributed to the stretching vibration of $(PO_3)^{2-}$ [24,25]. As shown in Fig. 1a, for PA-Al, the broad peak at 542 cm^{-1} was ascribed to the stretching vibration of the Al-O bond. It was observed that the characteristic absorption peak of P-OH disappeared, and the peak position of $(PO_3)^{2-}$ moved to a high wavenumber region and formed a wide absorption band, indicating the existence of interaction between PA molecules and Al^{3+} ions [20]. However, after the sample was dried at 80°C for 12 h, the characteristic peaks at 3410 and 1640 cm^{-1} in PA-Al did not disappear, suggesting that PA-Al contained crystal water or adsorbed water [26]. In Fig. 1, for PA-Fe, the characteristic peak at 516 cm^{-1} was ascribed to the stretching vibration of Fe-O, and the broad peak of P–OH at 2850 cm^{-1} disappeared. Meanwhile, the peak corresponding to $(PO_3)^{2-}$ also moved to the high wavenumber region. The above results indicated that PA-Al and PA-Fe were successfully prepared.
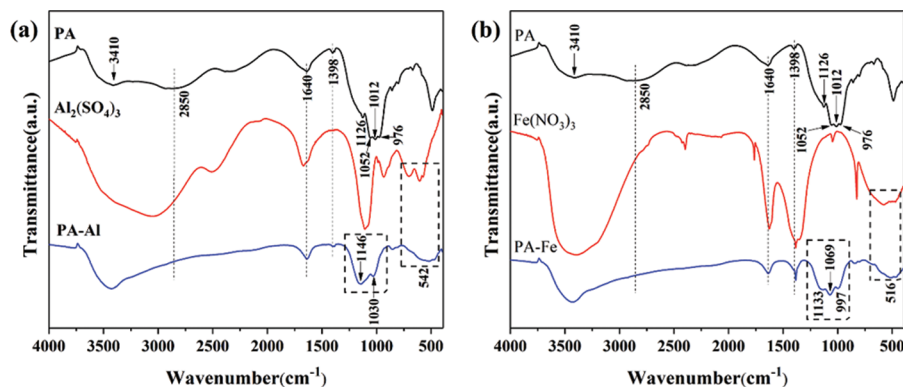

Figure 1: FTIR spectra of PA-Al (a) and PA-Fe (b)

The SEM-EDS was used to investigate the morphology and element distribution of PA-Al and PA-Fe. As shown in Fig. 2, both PA-Al and PA-Fe were exhibited irregularly shaped particles. As shown in Fig. 2a, four elements of C, O, P and Al existed in PA-Al, with P content of 5.72 at% and Al content of 4.08 at%, and the molar ratio of P/Al was closed to 1.5, indicating that the successful reaction between PA and $Al_2(SO_4)_3 \cdot 18H_2O$. In Fig. 2b, the molar ratio of P/Fe was 1.45, indicating that the PA solution also fully

reacted with $Fe(NO_3)_3 \cdot 9H_2O$ [27]. At the same time, it could be observed from EDS element mapping images that all elements in PA-Al and PA-Fe were evenly distributed, indicating the successful fabrication of PA-Al and PA-Fe.
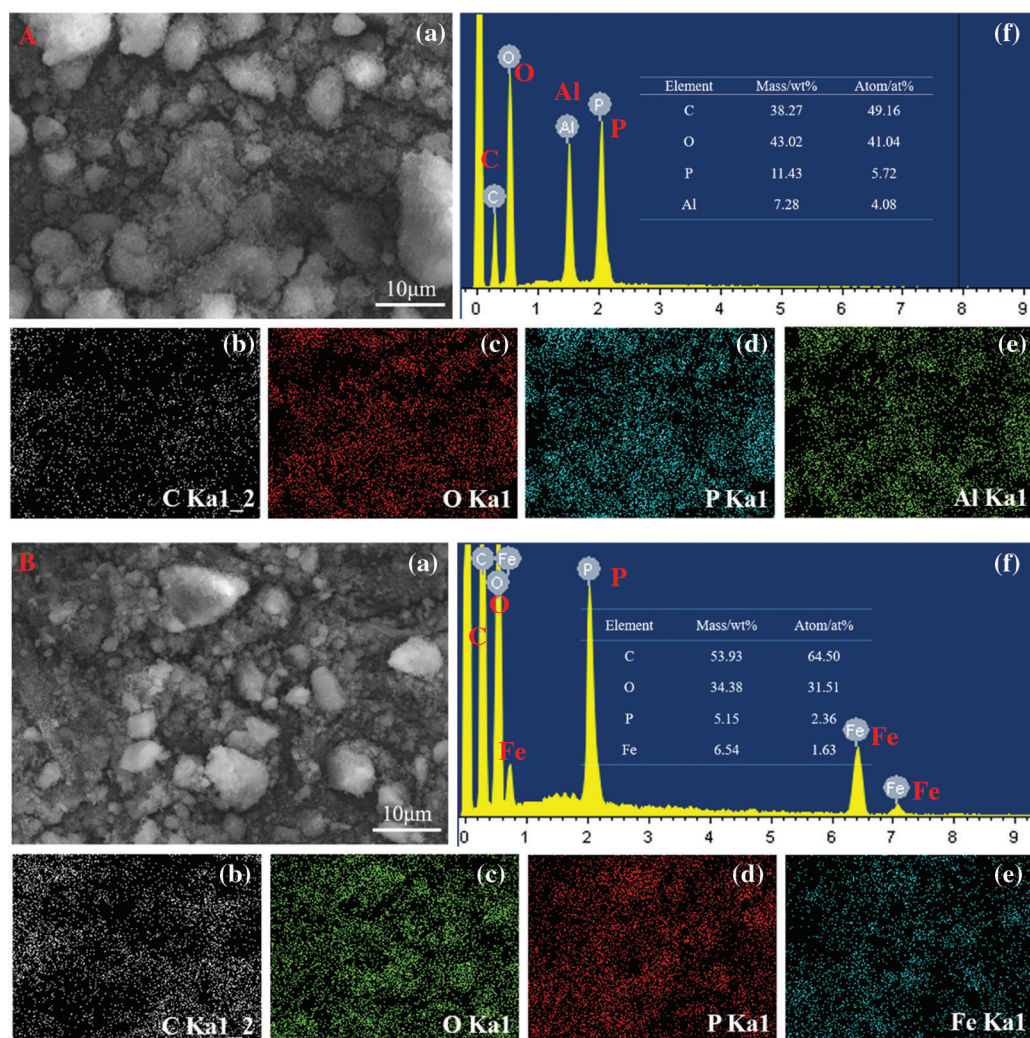

Figure 2: SEM and EDS element mapping images of PA-Al and PA-Fe: A(PA-Al); B(PA-Fe)

XRD patterns of PA-Al and PA-Fe were shown in Fig. 3. At the range of 20° to 40°, a broad peak in the pattern of PA-Al and PA-Fe was observed, suggesting a low crystal degree of PA-Al and PA-Fe, which were inconsistent with the previous report [28].

The degradation behavior of PA-Al and PA-Fe in the nitrogen atmosphere were analyzed by TGA and the correlation curves were displayed in Fig. 4. According to the figure, there were three stages in the degradation process of PA-Al and PA-Fe. The first stage at 40–200°C corresponded to the evaporation of water in PA-Al and PA-Fe. The second stage was at 200–420°C, PA was decomposed into polyphosphate and H_3PO_4. At the third stage, polyphosphate was decomposed into phosphorus-containing oxides [29]. At 700°C, the char residues of PA-Al and PA-Fe were 60.47 and 69.81 wt%, respectively.
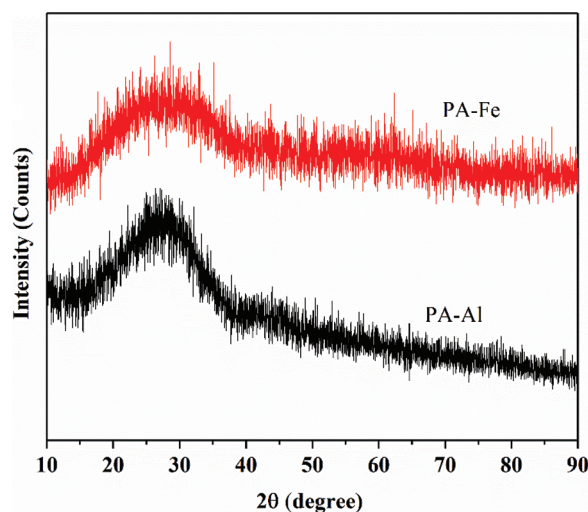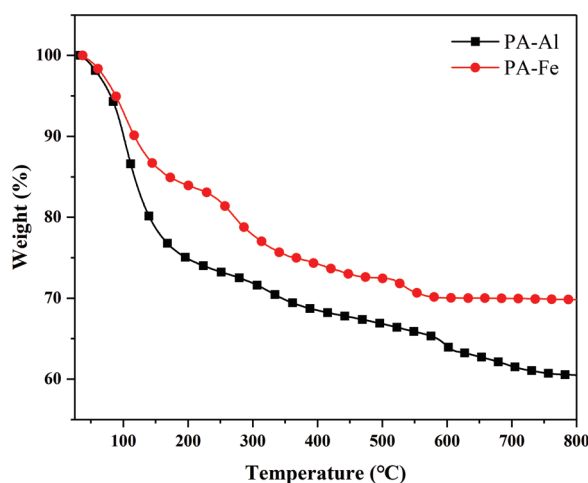
Figure 3: XRD pattern of PA-Al and PA-Fe

Figure 4: TGA curve of PA-Al and PA-Fe

3.2 Analysis of Cell Structure of RPUF Composites

The cell structure of RPUF, RPUF/PA-Al and RPUF/PA-Fe composites were shown in Fig. 5. According to Fig. 5a, the cells of pure RPUF were relatively uniform and the fracture surface was smooth. When 15 phr of PA-Al and PA-Fe were added, the cells of RPUF/PA-Al15 and RPPUF/PA-Fe15 composites increased and the cell size decreased, indicating that PA-Al and PA-Fe possessed certain nucleation effect, which could effectively reduce the free energy required by the nucleation process of foaming [30]. When magnified by 500 times, the smooth fracture surface of the composites could be observed, suggesting excellent compatibility between PA-Al/PA-Fe particles and the RPUF matrix. RPUF/PA-Al30 and RPUF/PA-Fe30 exhibited thinner cell walls with increased heterogeneity of cell structure when more flame retardants were added. It was even observed obvious collapse of cell structure in RPUF/PA-Al30. This may be because PA could promote the foaming process, the active −OH in PA reacted with –N=C=O group in polyisocyanate to generate carbamate, which further decomposed and released CO_2, resulting in uneven forces in all directions during the growth of bubbles in the foaming process [31].
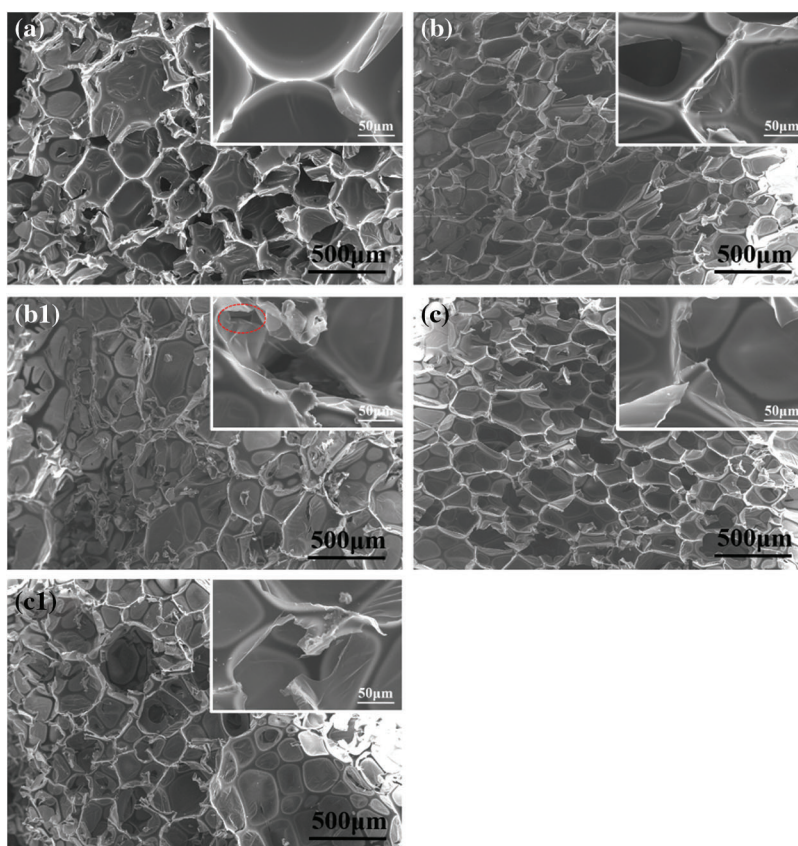
Figure 5: Cell structure of RPUF composites: (a) RPUF; (b) RPUF/PA-Al15; (b1) RPUF/PA-Al30; (c) RPUF/PA-Fe15; (c1) RPUF/PA-Fe30

3.3 Physical Properties of RPUF Composites

Apparent density as the important parameters, which affects the thermal, mechanical and physical properties of polymers. It directly affects the application for RPUF composites [32]. It could be seen from Table 2, pure RPUF possessed a density of 54.9 kg/m³. With the increase of PA-Al or PA-Fe content, the density of the composites decreased obviously, which was because PA-Al and PA-Fe promoted foaming and nucleation. As observed from Table 2, pure RPUF possessed a thermal conductivity of 0.0390 W/m·K. With the addition of PA-Al or PA-Fe, the thermal conductivity of RPUF/PA-Al15, RPUF/PA-Fe15 and RPUF/PA-Fe30 composites had little change compared with pure RPUF. However, the thermal conductivity of RPUF/PA-Al30 increased to 0.0425 W/m·K, which may be due to the addition of PA-Al30 resulting in the destruction of the closed cell structure [33].

3.4 Flame Retardancy of RPUF Composites

The LOI and horizontal combustion were used to evaluate the flame retardancy of the composites, and the corresponding test results were given in Table 3. The LOI value pure RPUF was 18.8 vol%, the horizontal combustion rate was 319.15 mm·min⁻¹, which was accompanied by dripping. With the increase of PA-Al or PA-Fe content, the LOI value of RPUF composites was enhanced. Meanwhile, the horizontal combustion rate of RPUF composites was decreased significantly. Therefore, Pa-Al and PA-Fe played a positive role in improving the flame retardancy of RPUF composites.

Table 2: Typical physical performance parameters of RPUF composites

Sample	$\rho/(kg/m^3)$	$\lambda/(W/m \cdot K)$
RPUF	54.9 ± 3.1	0.0390 ± 0.0004
RPUF/PA-Al15	44.8 ± 2.4	0.0382 ± 0.0006
RPUF/PA-Al30	43.0 ± 2.7	0.0425 ± 0.0008
RPUF/PA-Fe15	48.7 ± 4.2	0.0392 ± 0.0004
RPUF/PA-Fe30	41.3 ± 1.3	0.0389 ± 0.0003

Table 3: LOI, horizontal burning of RPUF composites

Sample	LOI/vol%	Horizontal burning		
		t/s	L/mm	Rating/mm·min^{-1}
RPUF	18.8	14.10	75	319.15
RPUF/PA-Al15	19.5	16.35	75	275.23
RPUF/PA-Al30	19.8	16.72	75	269.14
RPUF/PA-Fe15	20.2	18.78	75	239.62
RPUF/PA-30	20.4	19.54	75	230.30

Abbreviations: L, horizontal combustion length; t, horizontal burning time.

3.5 Thermal Stability of RPUF Composites

Fig. 6 and Table 4 were degradation curves and related data of RPUF, RPUF/PA-Al and RPUF/PA-Fe composites under nitrogen condition. The initial degradation temperature ($T_{-5\%}$) of pure RPUF was 254°C, and the degradation midpoint temperature ($T_{-50\%}$) was 338°C. There were three stages in the degradation process of RPUF, and the T_{max} corresponding to the temperature at maximum degradation rate in each stage was 291°C, 335°C and 460°C, respectively. The first and second stages in the range of 210–400°C, the hard segment of RPUF molecular chain was degraded, releasing isocyanates, aldehydes, alcohols, primary or secondary amines, olefins, H_2O and CO_2. Then the oxidative decomposition of isocyanates and aromatic compounds occurred in the third stage of 400–550°C with the formation of CO [34–36]. The char residues of RPUF was only 12.4 wt% when heated to 700°C. RPUF/PA-Al15 and RPUF/PA-Fe15 both had a lower $T_{-5\%}$ than pure RPUF, indicating that the addition of PA-Al/PA-Fe promoted the initial degradation of polyurethane molecular chains. It is worth noting that when 30 phr PA-Al or PA-Fe were added, the degradation stage of the composite was changed into two stages, and the degradation rate was significantly reduced. Moreover, $T_{-50\%}$ and T_{max} values had been greatly improved. This is due to the branching and cross-linking reactions of pyrophosphate and polyphosphate generated by the decomposition of PA-Al/PA-Fe [24], which catalyzed the dehydration carbonization of RPUF molecules. It could form a stable protective char layer, which inhibited the degradation of the composites, and made the degradation of the hard segment within 210°C–400°C became a stage. RPUF/PA-Al30 and RPUF/PA-Fe30 composites at 700°C possessed the char residues of 20.7 and 22.1 wt%, respectively, which were significantly higher than those of unmodified RPUF. The above results indicated that PA-Al/PA-Fe could promote the initial degradation of the RPUF composites and cross-link with the polyurethane matrix at medium and high temperatures to form a protective barrier, thereby improving the high-temperature thermal stability of the composites.
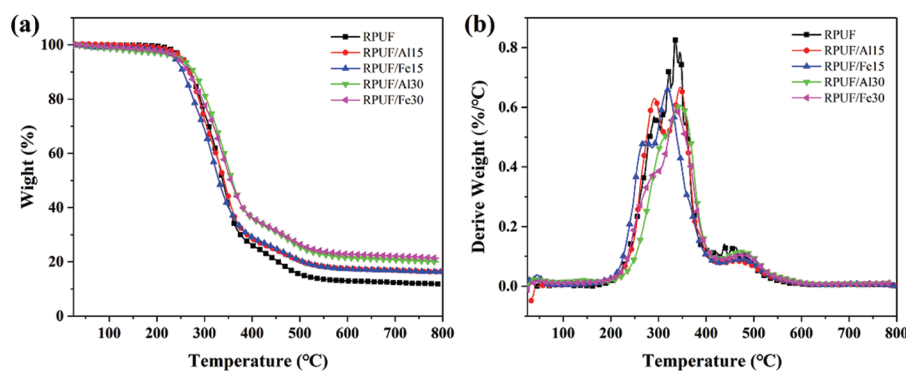
Figure 6: TGA (a) and DTG (b) curves of RPUF composites

Table 4: TGA data of RPUF composites

Sample	$T_{-5\%}$(°C)	$T_{-50\%}$(°C)	T_{max}(°C)			Char residue at 700°C (wt%)
			Step 1	Step 2	Step 3	
RPUF	254	338	291	335	460	12.4
RPUF/PA-Al15	253	341	292	346	462	16.9
RPUF/PA-Al30	249	358	–	346	473	20.7
RPUF/PA-Fe15	237	330	271	319	474	16.8
RPUF/PA-Fe30	245	355	–	337	478	22.1

3.6 Combustion Properties of RPUF Composites

Conical calorimetry is one of the most effective ways to analyze the combustion properties of various polymer materials [37]. The effect of PA-Al/PA-Fe on the combustion parameters of RPUF composites was shown in Fig. 7 and Table 5. As shown in the Fig. 7, due to the organic material and porous structure of the composites, the ignition time (TTI) of all samples was 2–3 s. As shown in Fig. 7a, RPUF burned rapidly and reached the peak heat release rate (pHRR) of 260.7 kW/m^2 at 49 s. When 30 phr PA-Al or PA-Fe was added, the pHRR of RPUF/PA-Al30 and RPUF/PA-Fe30 composites decreased to 248.4 and 254.4 kW/m^2, respectively, which may be due to the catalytic carbonization effect of PA-Al/PA-Fe [20,38]. According to Fig. 7b, RPUF possessed a total heat release (THR) of 23.0 MJ/m^2. With the addition of PA-Al/PA-Fe, the THR of the composites was significantly decreased. THR value of RPUF/PA-Al30 exhibited 19.1 MJ/m^2, which was the lowest THR and 17.0% lower than unmodified RPUF. It was because that PA molecules could produce active free radicals capturing H· and ·OH free radicals produced by the pyrolysis of polyurethane molecular chains in the combustion process of composites, which inhibited the formation of flammable components and thus reduced the heat generated by combustion [39]. At the same time, the addition of PA-Al/PA-Fe decreased the continuous combustion time (T_d) of the composites. The T_d of RPUF/PA-Al30 was 116 s, showing a strong self-extinction of the composites in combustion. The results confirmed that the fire safety of the composites was significantly improved when PA-Al and PA-Fe were loaded.

The smoke generation rate (SPR), total smoke release (TSR) and smoke factor (SF: the product of pHRR and TSR) were used to measure the effect of PA-Al/PA-Fe on smoke generation and release during combustion of composites [40]. It could be seen from Fig. 7c, the SPR curves of RPUF/PA-Al30 and RPUF/PA-Fe30 composites were basically coincident with that of pure RPUF before reaching the peak. After reaching the peak value, the SPR curves of the composites decreased rapidly, and both of them were below the SPR

curve of RPUF. The results showed that the degradation products polyphosphate and metaphosphate of PA-Al/PA-Fe could promote the dehydration carbonization of polyurethane molecular chains, formed a stable protective char layer, and effectively reduced the escape of smoke particles in the combustion process of the composites. At the same time, the existence of metal ions also largely inhibited the generation of flue gas [20]. According to Figs. 7d and 7e and Table 5, the TSR and SF of RPUF were 422.6 m^2/m^2 and 110.2 MW/m^2, respectively. Compared with pure RPUF, the TSR and SF of RPUF/PA-Al30 decreased by 22.0% and 25.7%, respectively, suggesting excellent smoke suppression performance.
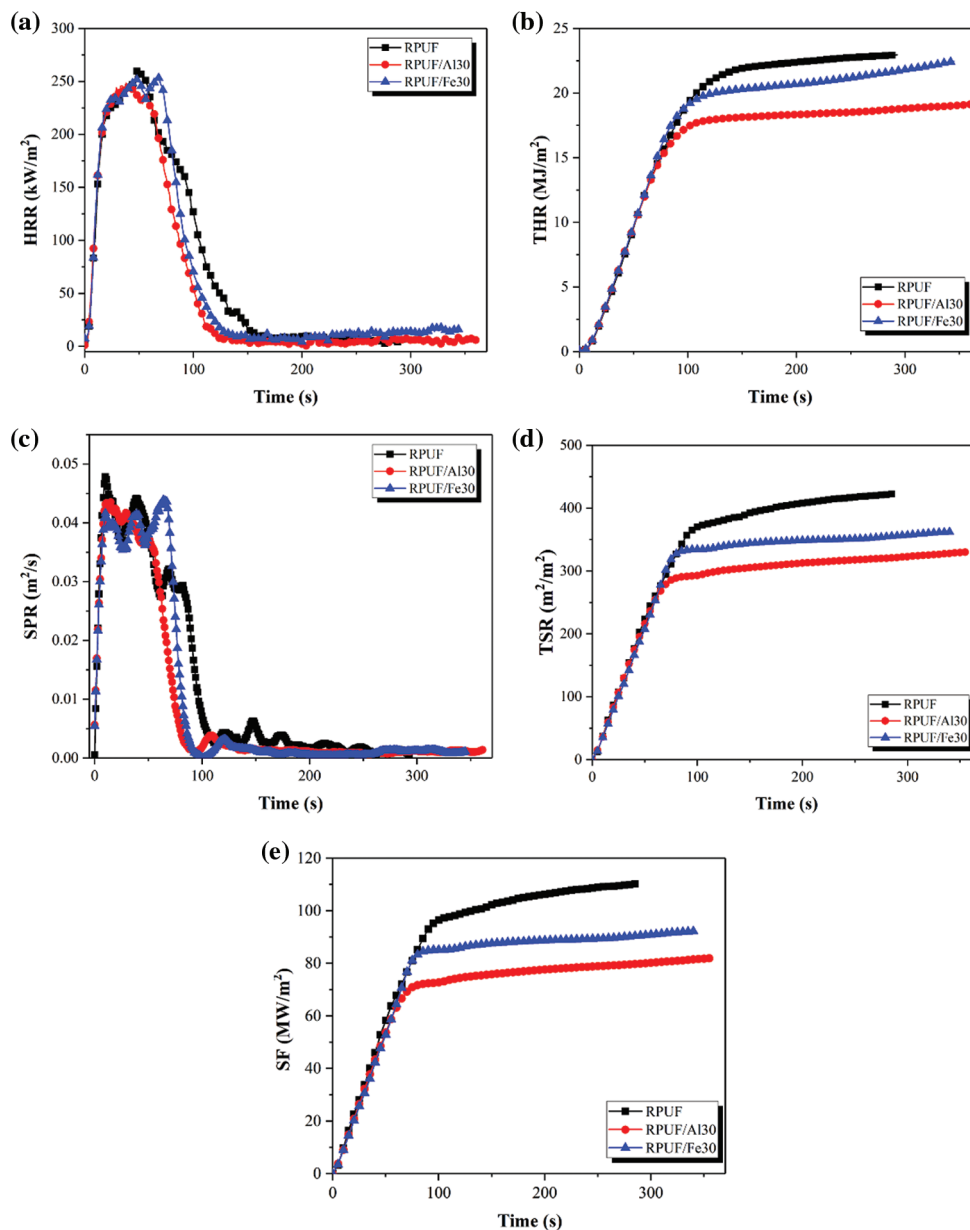

Figure 7: HRR, THR, SPR, TSR and SF curves of RPUF composites: (a) HRR; (b) THR; (c) SPR; (d) TSR; (e) SF

Table 5: Cone calorimetric data of RPUF composites

Sample	TTI (s)	T_p (s)	T_d (s)	pHRR (kW/m^2)	THR (MJ/m^2)	TSR (m^2/m^2)	FPI (m^2·s/kW)	FGI (kW/m^2·s)	SF (MW/m^2)
RPUF	2	49	154	260.7	23.0	422.6	0.0077	5.32	110.2
RPUF/PA-Al30	2	37	116	248.4	19.1	329.8	0.0081	6.71	81.9
RPUF/PA-Fe30	3	64	126	254.4	22.5	362.2	0.0118	3.98	92.1

Furthermore, fire growth index (FGI, ratio of pHRR to peak time T_P) and fire performance index (FPI, ratio of TTI to pHRR) were applied to analyze the fire safety of RPUF composites [41]. As shown in Table 5, compared with RPUF, the FPI of RPUF/PA-Al30 and RPUF/PA-Fe30 were 0.0081 and 0.0118 m^2·s/kW, indicating lower fire hazard. Since the addition of PA-Al promoted the initial degradation of the composite and reduced the T_P value of RPUF/PA-Al30, the FGI of RPUF/PA-Al30 was slightly higher than that of RPUF.

3.7 Analysis of Gas-Phase Products of RPUF Composites

The gaseous products of RPUF, RPUF/PA-Al30 and RPUF/PA-Fe30 composites during pyrolysis were investigate by TG-FTIR to explore the flame retardant mechanism of PA-Al and PA-Fe. Fig. 8 showed that the temperature corresponding to the maximum release intensity of gaseous products for the composites was around 350°C. The peak values of gas-phase products were mainly distributed between 3550–3750, 2800–3050, 2250–2400, 1500–1800, 950–1200 and 650–750 cm^{-1}, which were in agreement with previous reports [31]. The FTIR spectra of the gaseous products of the composites at 350°C were shown in Fig. 9. The peaks at 3730, 2968, 2360, 1630 and 690 cm^{-1} corresponding to the characteristic peaks of N-H bonds in carbamates, hydrocarbons, isocyanates, aromatic compounds and HCN, respectively [42–45].
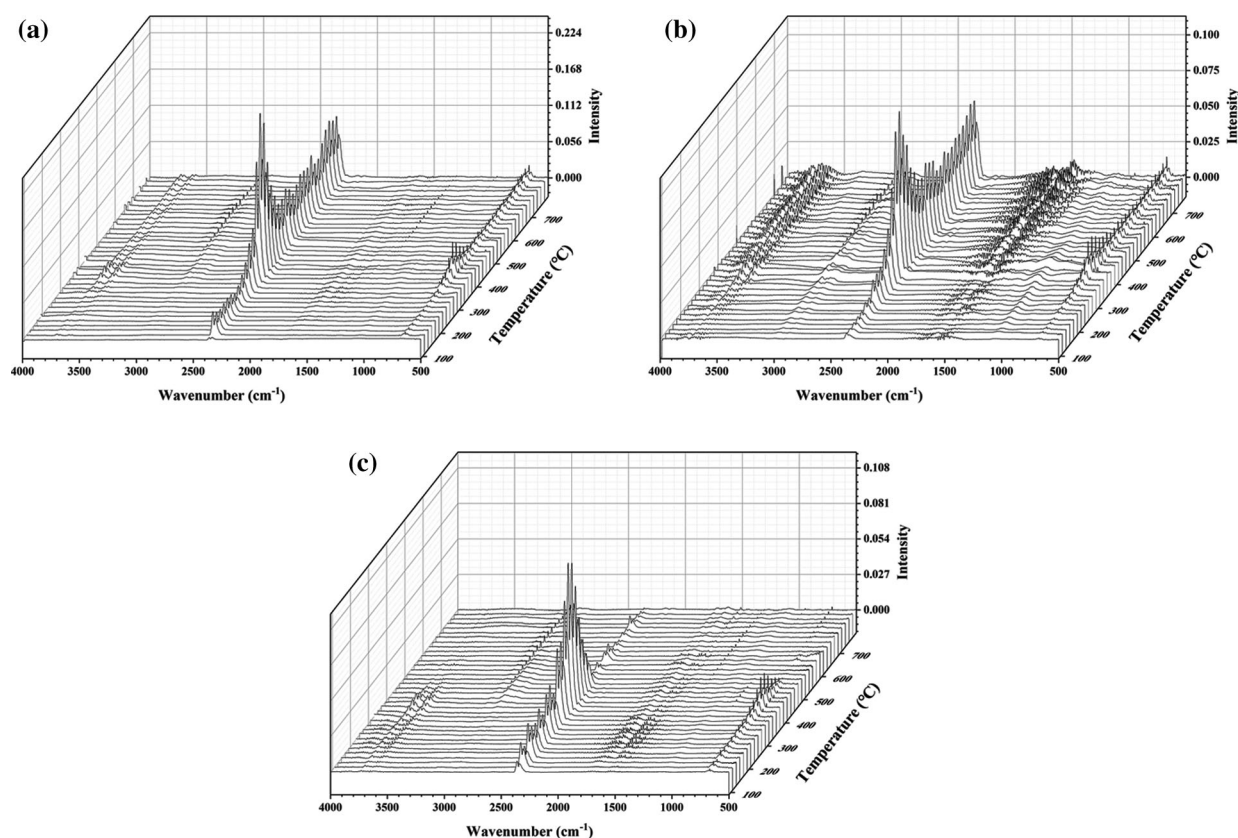

Figure 8: TG-FTIR 3D spectra of RPUF composites. (a) RPUF (b) RPUF/PA-A130 (c) RPUF/PA-Fe30
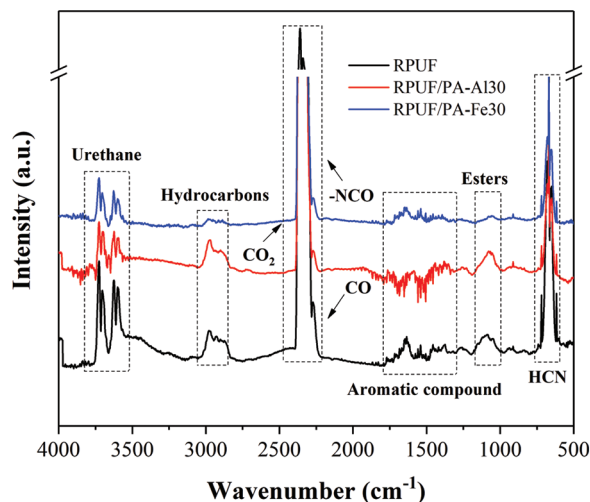
Figure 9: The FTIR spectrum of the pyrolysis product of RPUF composites at 350°C

According to Figs. 8 and 9, the volatile products of RPUA/PA-Al30 and RPUF/PA-Fe30 were consistent with those of RPUF. For quantitative comparison, Fig. 10 presented the release intensity *vs.* time curves for typical cracking gas-phase products of RPUF, RPUF/PA-Al30 and RPPUF/PA-Fe30. It could be observed that the release intensity of hydrocarbons for RPUF/PA-Al30 was higher than RPUF before 450°C, probably due to the initial decomposition of phytic acid in PA-Al, which promoted the degradation of the polyurethane molecular chain. At the same time, the early char layer of RPUF/PA-Al was unstable and further combustion led to the increase of hydrocarbon. For RPUF/PA-Fe30, compared with RPUF, the curves of each typical pyrolysis gas-phase product were below RPUF, indicating that PA-Fe inhibited the release of gas-phase products for RPUF/PA-Fe30 in the combustion process. This may be caused by the Lewis acid-base interaction between PA and the polyurethane molecular chain, which promoted pyrolysis products of polyurethane molecular chain into condensed phase to form compact char [46]. CO and HCN are important factors causing serious death in polyurethane fire [44,47]. The interaction of PA and metal ions in PA-Al/PA-Fe could effectively reduce the release of toxic gases during the degradation of RPUF/PA-Al and RPUF/PA-Fe composites. As shown from Figs. 10d and 10e, PRUF/PA-Fe30 exhibited the lowest CO and HCN production, suggesting an excellent detoxification effect of PA-Fe.

3.8 Char Residues Analysis of RPUF Composites

EDS mapping and SEM images of the char residues for the composites were gave in Fig. 11. It could be observed that the char residues of RPUF was loose and thin, with obvious cracks on the surface, which was unfavorable to restrain heat and mass transfer during combustion, resulting in more heat and smoke release. When 15 phr PA-Al or PA-Fe was added, the compactness of the char layer for the composite increased obviously, and the cracks almost disappeared, but there were still some holes on the surface of RPUF/PA-Al15. When the addition amount of PA-Al/PA-Fe reached 30 phr, RPUF/PA-Al30 and RPUF/PA-Fe30 composites exhibited compact char layers with vermicular structure after combustion, which was the result of the catalytic carbonization effect of PA and cross-linking effect of metal ions. The above structure was conducive to preventing the diffusion of flammable gas and toxic gas, inhibiting the heat transfer process in the combustion area to achieve the flame retardant purpose.

Further study on the element composition of the char layer of the composites showed that the char slag of RPUF mainly contained C, O and N elements. With the addition of PA-Al/PA-Fe, RPUF/PA-Al30 and RPUF/PA-Fe30 exhibited decreased N and O content with significantly increased C content in the char

residue, the enhanced C elements were conducive to the formation of stable graphite-carbon structure. Moreover, The C/O ratio of RPUF/PA-Al30 and RPUF/PA-Fe30 increased significantly compared with pure RPUF, meaning that RPUF/PA-Al30 and RPUF/PA-Fe30 composites possessed higher oxidation resistance and cross-linking density for the char layer [48]. Therefore, the composites had higher char residues and better smoke & toxicity suppression. At the same time, phosphorus and metal elements in RPUF/PA-Al30 and RPUF/PA-Fe30 contributed to the formation of the condensed char layer.
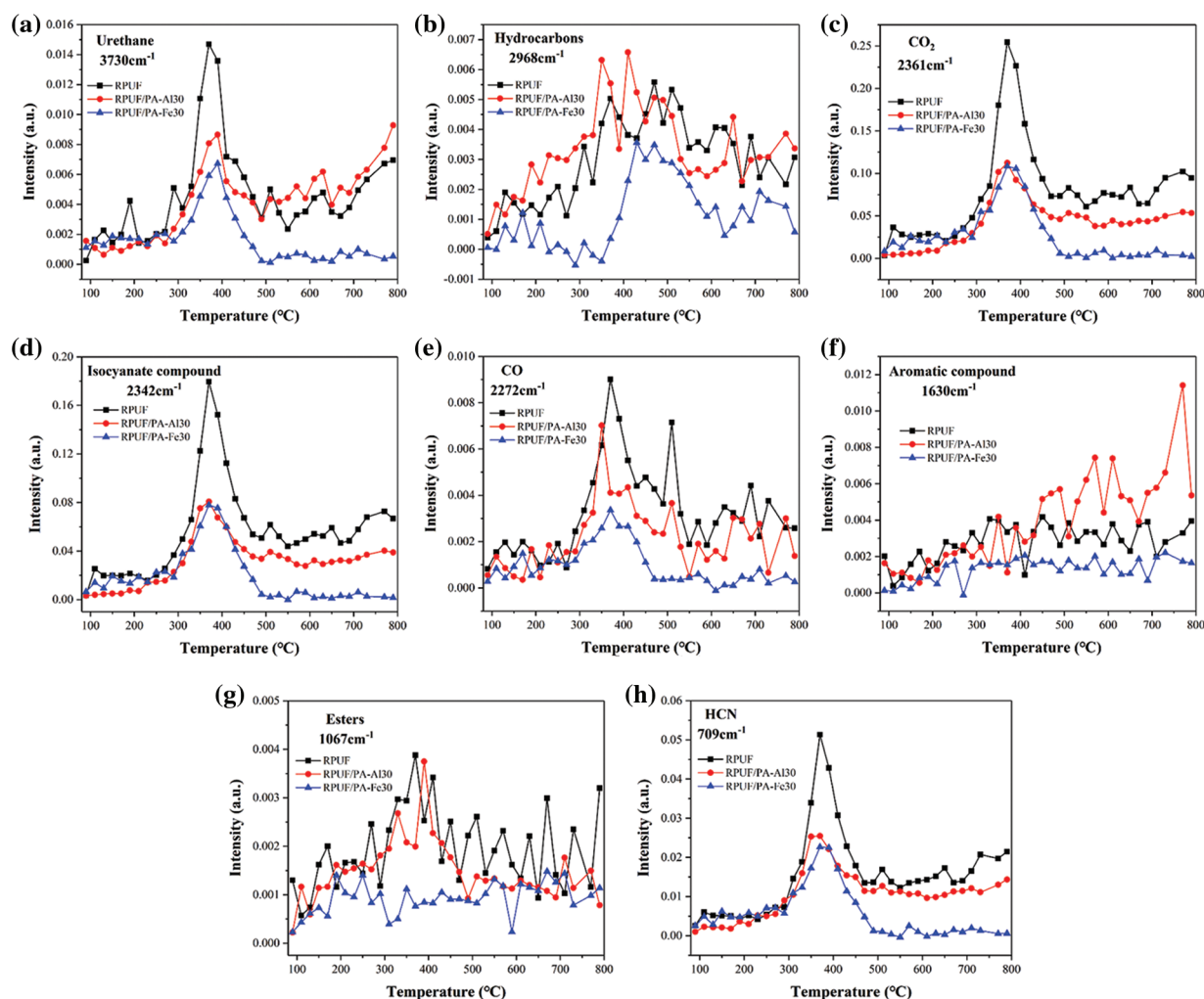

Figure 10: Curves of the typical cracking gas intensity of RPUF composites over time: (a) Urethane; (b) Hydrocarbons; (c) CO_2; (d) Isocyanate compound; (e) CO; (f) Aromatic compound; (g) Esters; (h) HCN

Raman spectra of char residues which was obtained in muffle furnace for the composites was shown in Fig. 12. The D peak at 1360 cm^{-1} corresponded to the amorphous phase composed of disordered carbon atoms, and the G peak at 1580 cm^{-1} corresponded to the graphited carbon atoms in the crystalline phase. The graphitization degree of char residues could be measured by the area ratio of D peak to G peak (I_D/I_G). The smaller the ratio was, the higher the graphitization degree was, the higher the thermal stability and flame retardancy of the composites were [49–51]. It could be observed that I_D/I_G of char residues for RPUF was 2.55. For RPUF/PA-Al or RPUF/PA-Fe composites, the char residues decreased with

PA-Al/PA-Fe loading, indicating that the addition of PA-Al/PA-Fe helped to improve the graphitization degree of char residues for the composites, endowing them with enhanced thermal resistance.
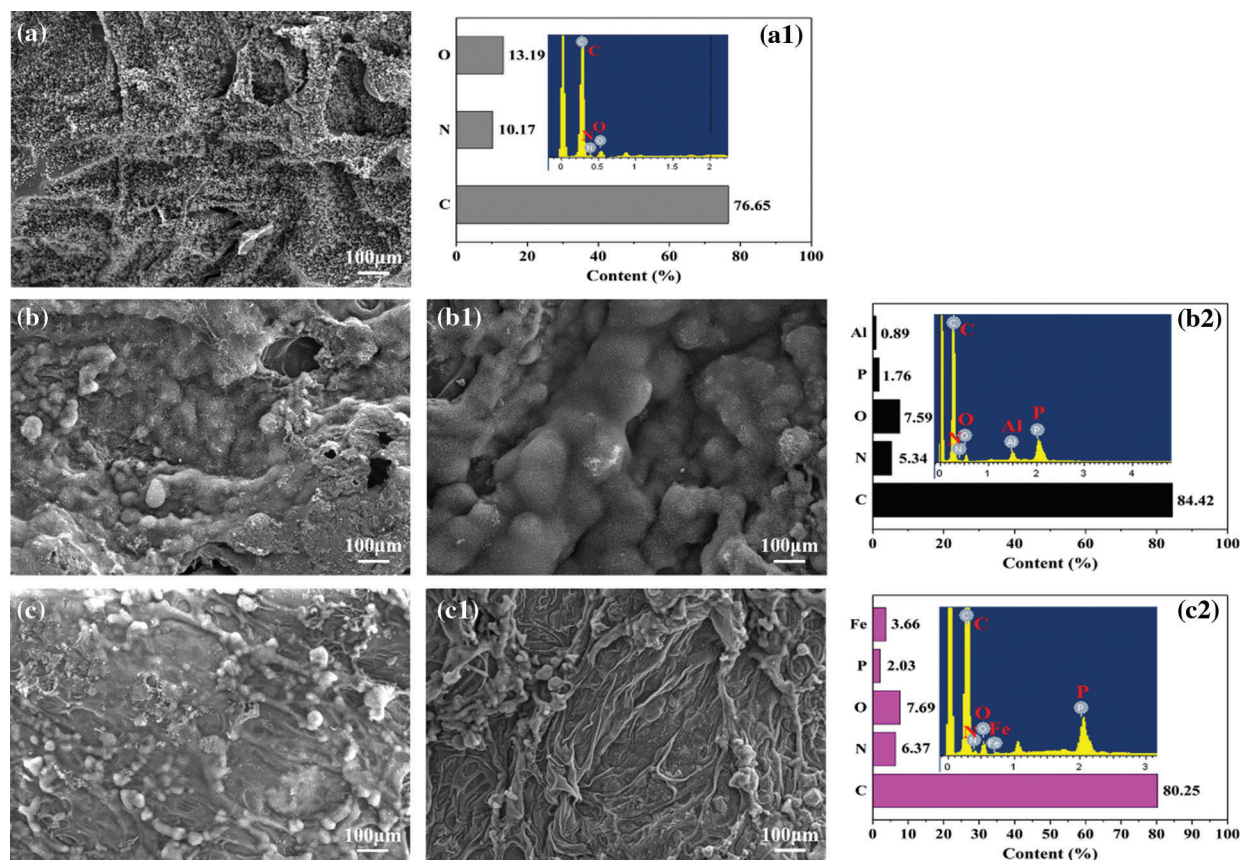

Figure 11: SEM images and EDS analysis of char residues for RPUF composites: (a, a1) RPUF; (b) RPUF/PA-Al15; (b1, b2) RPUF/PA-Al30; (c) RPUF/PA-Fe15; (c1, c2) RPUF/PA-Fe30

3.9 Flame Retardant Mechanism

Combined with the above analysis, the flame retardant mechanism of RPUF/PA Fe composites was proposed in Fig. 13. In the condensed phase, pyrophosphate and polyphosphate produced by PA-Fe decomposition could catalyze the pyrolysis products of the composites to form condensed phase carbon and reduced the release of combustibles & toxic gas. At the same time, PA molecules could produce active free radicals capturing H· and OH free radicals in the combustion process of composites to block the combustion reaction. In addition, Fe-P species in the char layer also acted as an effective catalytic effect in the redox reaction during combustion, which was confirmed by the significant inhibition of reduced gas products (isocyanate compounds, aromatic compounds, CO and HCN) [38]. It can be concluded that PA-Fe plays an important role in flame retardant, smoke and toxicity suppression of RPUF composites.
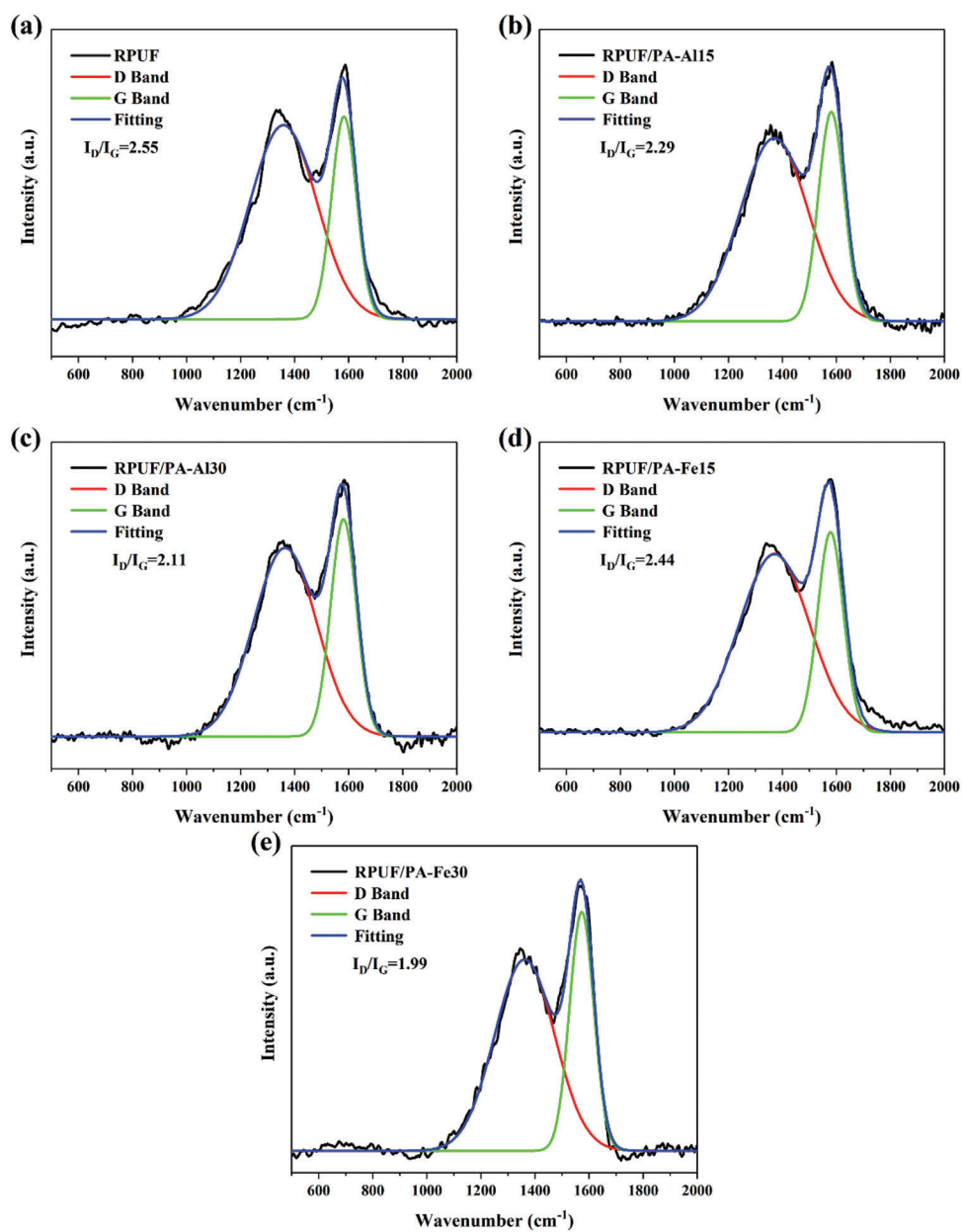
Figure 12: Raman spectra of RPUF composites: (a) RPUF; (b) RPUF/PA-Al15; (c) RPUF/PA-Al30; (d) RPUF/PA-Fe15; (e) RPUF/PA-Fe30
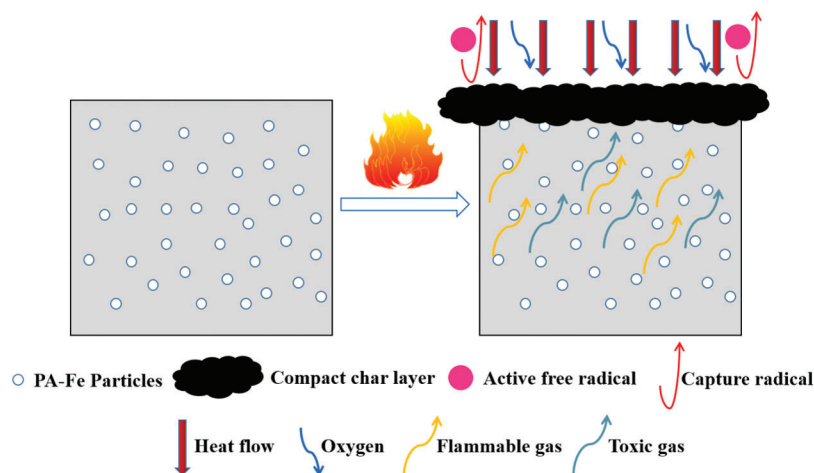
Figure 13: Schematic diagram of flame retardant mechanism (taking RPUF/PA-Fe composites as an example)

4 Conclusion

Bio-based flame retardants aluminum phytate (PA-Al) and iron phytate (PA-Fe) were fabricated by simple ionic reaction with phytic acid and metal salt as raw materials, which were used to prepare flame retardant RPUF composites. The addition of PA-Al/PA-Fe could decrease the apparent density of the composites. SEM test showed that PA-Al/PA-Fe exhibited excellent compatibility with the RPUF matrix. TGA and cone calorimetry tests confirmed that the addition of PA-Al/PA-Fe could enhance the thermal stability of the composites at high temperatures, which also endowed them with improved smoke suppression performance. At the same time, TG-FTIR suggested that PA-Fe exhibited better toxicity reduction properties compared with PA-Al. Compared with RPUF, PA-Fe had a positive effect on reducing the release intensity of flammable gases (hydrocarbons, esters) and toxic gases (isocyanate, CO, aromatic compounds, HCN) during the pyrolysis of composites. The above work provided a new strategy for the development and application of bio-based flame retardants.

Conflicts of Interest: The authors declare that they have no conflicts of interest to report regarding the present study.

References

1. Ju, Z. H., He, Q., Zhan, T. Y., Zhang, H. Y., Sun, L. et al. (2019). Steam exploded peanut shell fiber as the filler in the rigid polyurethane foams. *Journal of Polymer Research, 7(11),* 1077–1091. DOI 10.32604/jrm.2019.07525 .

2. Wang, Y. T., Wang, F., Dong, Q. X., Xie, M. C., Liu, P. et al. (2017). Core-shell expandable graphite @ aluminum hydroxide as a flame-retardant for rigid polyurethane foams. *Polymer Degradation and Stability, 146,* 267–276. DOI 10.1016/j.polymdegradstab.2017.10.017.

3. Tang, G., Jiang, H. H., Yang, Y. D., Chen, D. P., Liu, C. L. et al. (2020). Preparation of melamine-formaldehyde resin-microencapsulated ammonium polyphosphate and its application in flame retardant rigid polyurethane foam composites. *Journal of Polymer Research, 27(12),* 375. DOI 10.1007/s10965-020-02343-7.

4. Huang, Y. B., Jiang, S. H., Liang, R. C., Liao, Z. W., You, G. X. (2019). A green highly-effective surface flame-retardant strategy for rigid polyurethane foam: Transforming UV-cured coating into intumescent self-extinguishing layer. *Composites Part A: Applied Science and Manufacturing, 125,* 105534. DOI 10.1016/j.compositesa.2019.105534.

5. Liu, C., Zhang, P., Shi, Y. Q., Rao, X. H., Cai, S. C. et al. (2020). Enhanced fire safety of rigid polyurethane foam via synergistic effect of phosphorus/nitrogen compounds and expandable graphite. *Molecules, 25(20),* 4741. DOI 10.3390/molecules25204741.

6. Akdogan, E., Erdem, M., Ureyen, M. E., Kaya, M. (2020). Rigid polyurethane foams with halogen-free flame retardants: Thermal insulation, mechanical, and flame retardant properties. *Journal of Applied Polymer Science, 137(1),* 47611. DOI 10.1002/app.47611.

7. Zhang, G. Y., Lin, X. Q., Zhang, Q. Q., Jiang, K. S., Chen, W. S. et al. (2020). Anti-flammability, mechanical and thermal properties of bio-based rigid polyurethane foams with the addition of flame retardants. *RSC Advances, 10(53),* 32156–32161. DOI 10.1039/D0RA06561G.

8. Yang, W., Yuen, R., Hu, Y., Lu, H. D., Song, L. (2011). Development and characterization of fire retarded glass-fiber reinforced poly (1,4-butylene terephthalate) composites based on a novel flame retardant system. *Industrial & Engineering Chemistry Research, 50(21),* 11975–11981. DOI 10.1021/ie201550z.

9. Chai, H., Duan, Q. L., Jiang, L., Sun, J. H. (2019). Effect of inorganic additive flame retardant on fire hazard of polyurethane exterior insulation material. *Journal of Thermal Analysis and Calorimetry, 135(5),* 2857–2868. DOI 10.1007/s10973-018-7797-3.

10. Zhang, J. H., Kong, Q. H., Wang, D. Y. (2018). Simultaneously improving the fire safety and mechanical properties of epoxy resin with Fe-CNTs via large-scale preparation. *Journal of Materials Chemistry A, 6(15),* 6376–6386. DOI 10.1039/C7TA10961J.

11. Abolins, A., Pomilovskis, R., Vanags, E., Mierina, I., Michalowski, S. et al. (2021). Impact of different epoxidation approaches of tall oil fatty acids on rigid polyurethane foam thermal insulation. *Materials, 14(4),* 894. DOI 10.3390/ma14040894.

12. Laoutid, F., Vahabi, H., Shabanian, M., Aryanasab, F., Zarrintaj, P. et al. (2018). A new direction in design of bio-based flame retardants for poly(lactic acid). *Fire and Materials, 42(8),* 914–924. DOI 10.1002/fam.2646.

13. Kerche, E. F., Bock, D. N., Delucis, R., Magalhes, W., Amico, S. C. (2021). Micro fibrillated cellulose reinforced bio-based rigid high- density polyurethane foams. *Cellulose, 28(7),* 4313–4326. DOI 10.1007/s10570-021-03801-1.

14. Yang, R., Wang, B., Li, M. D., Zhang, X., Lin, J. C. (2019). Preparation, characterization and thermal degradation behavior of rigid polyurethane foam using a malic acid based polyols. *Industrial Crops and Products, 136,* 121–128. DOI 10.1016/j.indcrop.2019.04.073.

15. Gao, L. P., Zhen, G. Y., Zhou, Y. H., Hu, L. H., Feng, G. D. (2015). Improved mechanical property, thermal performance, flame retardancy and fire behavior of lignin-based rigid polyurethane foam nanocomposite. *Journal of Thermal Analysis and Calorimetry, 120(2),* 1311–1325. DOI 10.1007/s10973-015-4434-2.

16. Septevani, A. A., Evans, D., Chaleat, C. M., Martin, D. J., Annamalai, P. K. (2015). A systematic study substituting polyether polyol with palm kernel oil based polyester polyol in rigid polyurethane foam. *Industrial Crops and Products, 66,* 16–26. DOI 10.1016/j.indcrop.2014.11.053.

17. Tsuyumoto, I., Miura, Y., Nirei, M., Ikurumi, S., Kumagai, T. (2011). Highly flame retardant coating consisting of starch and amorphous sodium polyborate. *Journal of Materials Science, 46(16),* 5371–5377. DOI 10.1007/s10853-011-5475-y.

18. Tsuyumoto, I. (2021). Flame-retardant coatings for rigid polyurethane foam based on mixtures of polysaccharides and polyborate. *Journal of Coatings Technology and Research, 18(1),* 155–162. DOI 10.1007/s11998-020-00390-9.

19. Marolt, G., Griar, E., Pihlar, B., Kolar, M. (2020). Complex formation of phytic acid with selected monovalent and divalent metals. *Frontiers in Chemistry, 8,* 582746. DOI 10.3389/fchem.2020.582746.

20. Cheng, L. Y., Wu, W. H., Meng, W. H., Xu, S., Han, H. D. et al. (2018). Application of metallic phytates to poly (vinyl chloride) as efficient biobased phosphorous flame retardants. *Journal of Applied Polymer Science, 135(33),* 46601. DOI 10.1002/app.46601.

21. Gao, Y. Y., Deng, C., Du, Y. Y., Huang, S. C., Wang, Y. Z. (2019). A novel bio-based flame retardant for polypropylene from phytic acid. *Polymer Degradation and Stability, 161,* 298–308. DOI 10.1016/j.polymdegradstab.2019.02.005.

22. Dong, J., Wen, Y., Miao, Y., Xie, Z. J., Zhang, Z. R. et al. (2010). A nanoporous zirconium phytate film for immobilization of redox protein and the direct electrochemical biosensor. *Sensors and Actuators B-Chemical, 150(1),* 141–147. DOI 10.1016/j.snb.2010.07.029.

23. Gao, X., Zhao, C. C., Lu, H. F., Gao, F., Ma, H. Y. (2014). Influence of phytic acid on the corrosion behavior of iron under acidic and neutral conditions. *Electrochimica Acta, 150,* 188–196. DOI 10.1016/j.electacta.2014.09.160.

24. Wang, P. J., Liao, D. J., Hu, X. P., Pan, N., Li, W. X. et al. (2019). Facile fabrication of biobased PNC-containing nano-layered hybrid: Preparation, growth mechanism and its efficient fire retardancy in epoxy. *Polymer Degradation and Stability, 159,* 153–162. DOI 10.1016/j.polymdegradstab.2018.11.024.

25. Valappil, S. P., Ready, D., Neel, E. A. A., Pickup, D. M., Chrzanowski, W. et al. (2008). Antimicrobial gallium-doped phosphate-based glasses. *Advanced Functional Materials, 18(5),* 732–741. DOI 10.1002/adfm.200700931.

26. Xue, Z. M., Zhang, Y. W., Li, G. F., Wang, J. F., Zhao, W. C. et al. (2016). Niobium phytate prepared from phytic acid and Nbcl5: A highly efficient and heterogeneous acid catalyst. *Catalysis Science & Technology, 6(4),* 1070–1076. DOI 10.1039/C5CY01123J.

27. Ma, D., Zhao, P. H., Li, J. (2017). Effects of zinc phytate on flame retardancy and thermal degradation behaviors of intumescent flame-retardant polypropylene. *Polymer-Plastics Technology and Engineering, 56(11),* 1167–1176. DOI 10.1080/03602559.2016.1255754.

28. Zhang, T., Yan, H. Q., Shen, L., Fang, Z. P., Zhang, X. M. et al. (2014). Chitosan/Phytic acid polyelectrolyte complex: A green and renewable intumescent flame retardant system for ethylene-vinyl acetate copolymer. *Industrial & Engineering Chemistry Research, 53(49),* 19199–19207. DOI 10.1021/ie503421f.

29. Shang, S., Yuan, B. H., Sun, Y. R., Chen, G. Q., Huang, C. Y. et al. (2019). Facile preparation of layered melamine-phytate flame retardant via supramolecular self-assembly technology. *Journal of Colloid and Interface Science, 553,* 364–371. DOI 10.1016/j.jcis.2019.06.015.

30. Liao, H. H., Liu, Y., Wang, Q., Duan, W. F. (2019). Preparation and properties of a poly(vinyl alcohol) hydrogel-melamine formaldehyde foam composite. *Polymer Composites, 40(5),* 2067–2075. DOI 10.1002/pc.24988.

31. Xiong, T. K., Zhou, X. Q., Zhang, M., Tang, H. T., Pan, Y. M. et al. (2021). Electrochemical-mediated fixation of CO_2: Three-component synthesis of carbamate compounds from CO_2, amines and N-alkenylsulfonamides. *Green Chemistry, 23,* 4328. DOI 10.1039/d1gc00949d.

32. Yang, R., Wang, B., Xu, L., Zhao, C. X., Zhang, X. et al. (2019). Synthesis and characterization of rigid polyurethane foam with dimer fatty acid-based polyols. *Polymer Bulletin, 76(7),* 3753–3768. DOI 10.1007/s00289-018-2570-0.

33. Wu, S., Deng, D., Zhou, L., Zhang, P., Tang, G. (2019). Flame retardancy and thermal degradation of rigid polyurethane foams composites based on aluminum hypophosphite. *Materials Research Express, 6(10),* 105365. DOI 10.1088/2053-1591/ab41b2.

34. Pang, X. Y., Chang, R., Weng, M. Q. (2018). Halogen-free flame retarded rigid polyurethane foam: The influence of titanium dioxide modified expandable graphite and ammonium polyphosphate on flame retardancy and thermal stability. *Polymer Engineering and Science, 58(11),* 2008–2018. DOI 10.1002/pen.24811.

35. Hu, Y. X., Zhou, Z. J., Li, S. S., Yang, D., Zhang, S. et al. (2021). Flame retarded rigid polyurethane foams composites modified by aluminum diethylphosphinate and expanded graphite. *Frontiers in Materials, 7,* 629284. DOI 10.3389/fmats.2020.629284.

36. Xu, Z. M., Duan, L. J., Hou, Y. B., Chu, F. K., Jiang, S. D. et al. (2020). The influence of carbon-encapsulated transition metal oxide microparticles on reducing toxic gases release and smoke suppression of rigid polyurethane foam composites. *Composites Part A: Applied Science and Manufacturing, 131,* 105815. DOI 10.1016/j.compositesa.2020.105815.

37. Kirpluks, M., Cabulis, U., Zeltins, V., Stiebra, L., Avots, A. (2014). Rigid polyurethane foam thermal insulation protected with mineral intumescent mat. *Autex Research Journal, 14(4),* 259–269. DOI 10.2478/aut-2014-0026.

38. Feng, X. M., Wang, X., Cai, W., Qiu, S. L., Hu, Y. et al. (2016). Studies on synthesis of electrochemically exfoliated functionalized graphene and polylactic acid/ferric phytate functionalized graphene nanocomposites as new fire hazard suppression materials. *ACS Applied Materials & Interfaces, 8(38),* 25552–25562. DOI 10.1021/acsami.6b08373.

39. Jiang, Z. L., Wang, C. S., Fang, S. Y., Ji, P., Wang, H. P. et al. (2018). Durable flame-retardant and antidroplet finishing of polyester fabrics with flexible polysiloxane and phytic acid through layer-by-layer assembly and sol-gel process. *Journal of Applied Polymer Science, 135(27),* 46414. DOI 10.1002/app.46414.

40. Chen, X. L., Zhuo, J. L., Song, W. K., Jiao, C. M., Qian, Y. et al. (2014). Flame retardant effects of organic inorganic hybrid intumescent flame retardant based on expandable graphite in silicone rubber composites. *Polymers for Advanced Technologies, 25(12),* 1530–1537. DOI 10.1002/pat.3397.

41. Zhao, L., Yuan, L., Liang, G. Z., Gu, A. J. (2015). Novel tough and thermally stable cyanate ester resins with high flame retardancy, low dielectric loss and constant based on a phenolphthalein type polyarylether sulfone. *RSC Advances, 5(73),* 58989–59002. DOI 10.1039/C5RA10670B.

42. Liu, X., Salmeia, K. A., Rentsch, D., Hao, J. W., Gaan, S. (2017). Thermal decomposition and flammability of rigid PU foams containing some DOPO derivatives and other phosphorus compounds. *Journal of Analytical and Applied Pyrolysis, 124,* 219–229. DOI 10.1016/j.jaap.2017.02.003.

43. Pagacz, J., Hebda, E., Michalowski, S., Ozirnek, J., Sternik, D. et al. (2016). Polyurethane foams chemically reinforced with POSS-thermal degradation studies. *Thermochimica Acta, 624,* 95–104. DOI 10.1016/j.tca.2016.09.006.

44. Xu, D. F., Yu, K. J., Qian, K. (2018). Thermal degradation study of rigid polyurethane foams containing tris (1-chloro-2-propyl) phosphate and modified aramid fiber. *Polymer Testing, 67,* 159–168. DOI 10.1016/j.polymertesting.2018.01.034.

45. Reinerte, S., Avotina, L., Zarins, A., Cabulis, U., Viksna, A. (2020). TG/Dta-FTIR as a method for analysis of tall oil based rigid polyurethane foam decomposition gaseous products in a low oxygen environment. *Polymer Degradation and Stability, 180,* 109313. DOI 10.1016/j.polymdegradstab.2020.109313.

46. Kaya, H., Ozdemir, E., Kaynak, C., Hacaloglu, J. (2016). Effects of nanoparticles on thermal degradation of polylactide/aluminium diethylphosphinate composites. *Journal of Analytical and Applied Pyrolysis, 118,* 115–122. DOI 10.1016/j.jaap.2016.01.005.

47. Jasiunas, L., McKenna, S. T., Bridiuvien, D., Miknius, L. (2020). Mechanical, thermal properties and stability of rigid polyurethane foams produced with crude-glycerol derived biomass biopolyols. *Journal of Polymers and the Environment, 28(5),* 1378–1389. DOI 10.1007/s10924-020-01686-y.

48. Xu, Z. S., Deng, N., Yan, L., Chu, Z. Y. (2018). Functionalized multiwalled carbon nanotubes with monocomponent intumescent flame retardant for reducing the flammability and smoke emission characteristics of epoxy resins. *Polymers for Advanced Technologies, 29(12),* 3002–3013. DOI 10.1002/pat.4420.

49. Shi, X. X., Jiang, S. H., Zhu, J. Y., Li, G. H., Peng, X. F. (2018). Establishment of a highly efficient flame-retardant system for rigid polyurethane foams based on bi-phase flame-retardant actions. *RSC Advances, 8(18),* 9985–9995. DOI 10.1039/C7RA13315D.

50. Zhou, K. Q., Liu, C. K., Gao, R. (2018). Polyaniline: A novel bridge to reduce the fire hazards of epoxy composites. *Composites Part A: Applied Science and Manufacturing, 112,* 432–443. DOI 10.1016/j.compositesa.2018.06.031.

51. Shi, Y. Q., Liu, C., Duan, Z. P., Yu, B., Liu, M. H. et al. (2020). Interface engineering of MXene towards super-tough and strong polymer nanocomposites with high ductility and excellent fire safety. *Chemical Engineering Journal, 399,* 125829. DOI 10.1016/j.cej.2020.125829.